Full-Scale Wind Tunnel Test of the McDonnell Douglas Five-Bladed Advanced Bearingless Rotor: Performance, Stability, Loads, Control Power, Vibration and HHC Data

Stephen A. Jacklin, Benton H. Lau, and Khanh Q. Nguyen
Aerospace Research Engineers
NASA Ames Research Center
Moffett Field, California

Roger L. Smith and Michael J. McNulty
Members of the Technical Staff
McDonnell Douglas Helicopter Company
Mesa, Arizona

Abstract

The McDonnell Douglas Helicopter Company (MDHC) and the NASA Ames Research Center jointly conducted a test of the McDonnell Douglas Advanced Rotor Technology (MDART) rotor in the Ames 40- by 80-Foot Wind Tunnel in 1992. The objective of that cooperative wind tunnel test program was to study the dynamic, aerodynamic, and aeroacoustic characteristics of an advanced bearingless rotor to obtain a comprehensive data base. The MDART testing at Ames produced a significant amount of performance, loads, and stability data up to 200 kt and thrusts of 1.8 g. This test was the first wind tunnel test of a full-scale, five-bladed, bearingless rotor. It was also the first test to apply higher harmonic control (HHC) to a full-scale bearingless rotor in order to study its effect on rotor vibration, loads, and noise. This paper summarizes the significant research findings for rotor performance, stability, loads, and vibration. A discussion of the effect of HHC on rotor vibration has been included.

Introduction

While the introduction of hingeless and bearingless rotors into the design of modern helicopters provides increased control moment and maneuverability, these rotors pose greater challenges to the dynamics and control systems engineers to accurately model the rotor system dynamics and predict their stability and loads characteristics. In an effort to obtain better predictive capabilities and to better understand bearingless rotor dynamics and loading characteristics, the McDonnell Douglas Helicopter Company (MDHC) and NASA Ames conducted a wind tunnel test program to study the MDHC advanced bearingless rotor concept. The five-bladed, bearingless rotor was a pre-production version of the MD Explorer helicopter rotor system. The rotor was tested over a wide range of operating conditions including speeds of up to 200 kt (μ=0.49) and thrusts over 10,000 lb (1g ~ 5,800 lb).

The planning of the wind tunnel testing began in 1989 with a critical need for test data needed to validate new bearingless rotor analytical capabilities. A joint wind tunnel test program was planned to provide these data. The project was named "McDonnell Douglas Advanced Rotor Technology" or MDART. The program was governed by a Memorandum of Understanding between NASA and McDonnell Douglas. The project goals were to obtain performance, loads, stability, and acoustic data for a state-of-the-art bearingless rotor system over a wide range of operating conditions, and also to measure the effects of open-loop higher harmonic control (HHC) inputs on these attributes.

Prior to initiation of the MDART program, NASA, McDonnell Douglas, and other helicopter manufacturers had been pursuing bearingless rotor technology. The first full-scale wind tunnel test of a four-bladed bearingless rotor was conducted at NASA Ames Research Center in the early 1980's [Ref. 1]. The modified BO-105 rotor tested, the Boeing BMR, was a damper-less design that used two back-to-back flexbeams per arm for blade retention and a torsionally-stiff torque tube to transmit pitch inputs to the blade. Although successfully tested to 165 kt, the rotor system was subject to structural load limits and low levels of in-plane damping difficulties which are greatly

Presented at the American Helicopter Society Aeromechanics Specialists Conference, San Francisco, California, January 19-21, 1994.

improved in the modern bearingless designs having snubber dampers and an external pitchcase.

The modern bearingless rotor design, now widely accepted, uses a single, centrifugally loaded flexbeam contained in a torsionally stiff pitchcase. The flexbeam provides blade retention and allows elastic blade root motion, while the pitchcase transfers blade pitch control moments from the pitch link to the blade. An elastomeric snubber/damper assembly reacts the shear load due to the pitch inputs, helps control the deflection of the flexbeam, and also provides lead-lag damping. This design approach has been successfully employed on the McDonnell Douglas HARP rotor, the Bell 680, the Bell 4BW Cobra [Ref. 2], the ECD BO-108 [Ref. 3], and, the most recent to fly, the McDonnell Douglas MD Explorer. This same rotor concept is also planned for use on the U.S. Army RAH-66 Comanche [Ref. 4].

At McDonnell Douglas, development of an advanced bearingless rotor design began as the Helicopter Advanced Rotor Program, or HARP. The HARP rotor was a four-bladed bearingless rotor which was successfully flown on a McDonnell Douglas MD 500 helicopter in 1985 at a wide range of flight conditions. This rotor employed the bearingless design as described above. Although the performance of the flexbeam was good, the cruciform shape of the cross section was difficult to manufacture and did not provide the desired service life improvement. A second generation HARP rotor was designed with flexbeams having a rectangular cross section and fiberglass rather than Kevlar construction. Fatigue testing of the flexbeam demonstrated exceptional rotor life. A 0.29-scale version of the new flexbeam and rotor was tested in the DNW wind tunnel in 1987 [Ref. 5].

Originally, it was planned to test a full-scale version of the second generation HARP rotor design in the Ames 40- by 80-Foot Wind Tunnel. However, due to the high cost for design and tooling of what would be a one-of-a-kind rotor, it was decided that the same research goals could be attained by testing the MD Explorer rotor (already in development using many of the technologies developed under the HARP rotor program). This effort required McDonnell Douglas to modify an existing rotor test stand for the MDART wind tunnel test program. This paper describes the test hardware, the MD Explorer rotor, and presents some of the rotor performance, stability, loads, and HHC-vibration data obtained during the 1992 wind tunnel test. Full documentation of the MDART test data is beyond

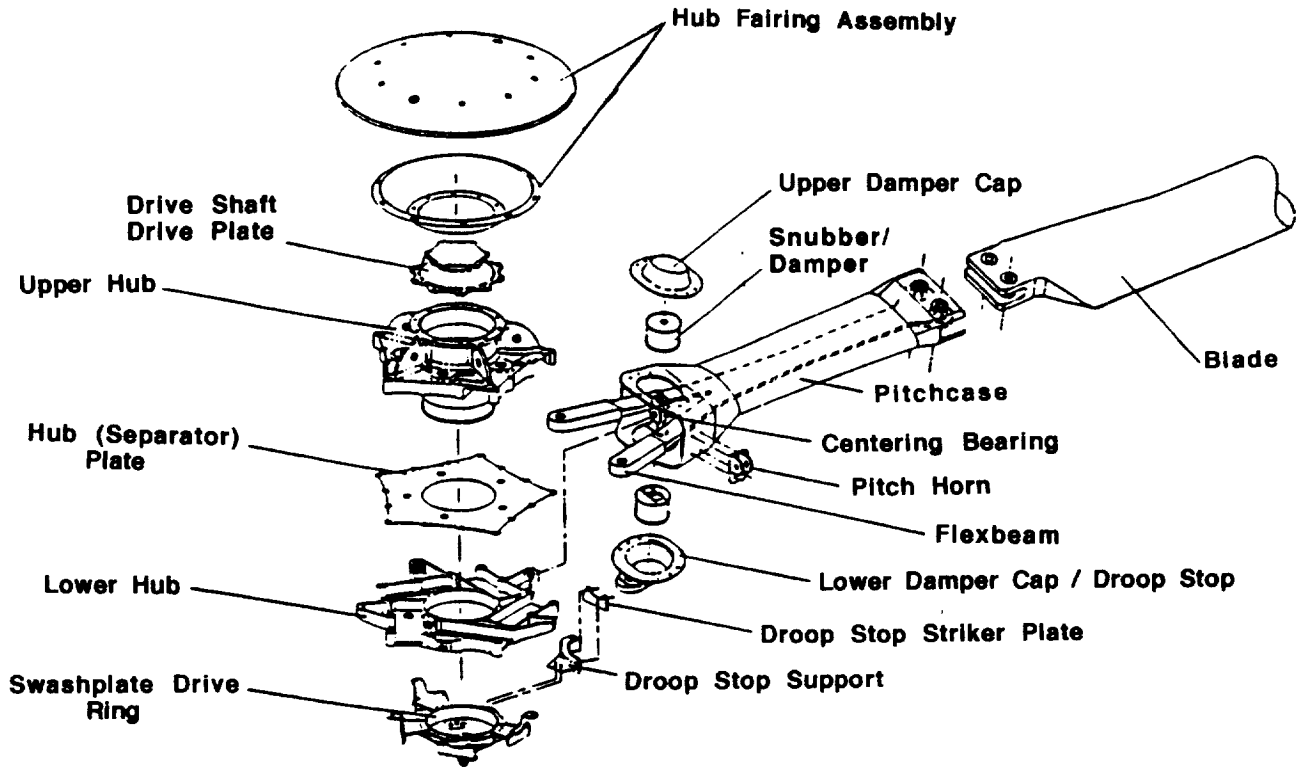

Figure 1. MDART rotor hub, flexbeam, pitchcase, and blade assembly.

the scope of this paper and is deferred to Ref. 6.

Hardware Description

MDART Rotor

The MDART rotor was essentially identical to the production MD Explorer main rotor, with the exception that weight saving machining on the aluminum hub was not done. A schematic of the rotor head is shown in Fig. 1. This five-bladed, bearingless rotor had a 16.9 ft radius and solidity of 0.075. The nominal 1g thrust for the rotor was taken to be 5800 lb for the MDART test. The key components of the rotor were the flexbeams, the pitchcases, the blades, and the snubber/damper assemblies. The leading and trailing legs of the flexbeams are mounted to the metallic hub such that the trailing edge arm of each flexbeam shares a retention bolt in common with the leading edge lug of the second flexbeam following it in an over/under arrangement.

The rotor blades were constructed with a S2 fiberglass spar, Nomex honeycomb core, and S2 fiberglass skin. The pitchcases, for which high stiffness was essential, were made of carbon/epoxy. The flexbeams were built of S2 fiberglass. The snubber/damper assembly consisted of upper and lower elastomeric dampers, each of which attached to the pitchcase and to the metal snubber. The snubber was attached to the hub via an elastomeric bearing. This bearing allowed pitch and flap rotations of the pitchcase relative to the hub. The snubber restricted the vertical displacement of the pitchcase root. This, together with the high pitchcase flapping stiffness, forced the virtual flapping hinge to be very near the snubber location for any flight condition. The high pitchcase chordwise stiffness, the carefully tailored chordwise stiffness of the flexbeam, and the relative softness of the elastomeric damper combined to yield a large amount of damper shearing motion per degree of blade lead-lag deflection. The damping force that resulted from shearing the high-loss-factor elastomer effectively stabilized the rotor.

The rotor is shown in Fig. 2. The blades used the McDonnell Douglas HH-10 airfoil section inboard and the HH-06 airfoil outboard, and had a linear twist of -10 deg. The blade tips had a parabolic leading edge sweep (22 deg at the tip) and a 2:1 taper ratio. The rotor nominal rotation speed was 392 RPM, producing a tip-speed of 695 ft/s. At 5800 lb thrust, the rotor thrust coefficient normalized by

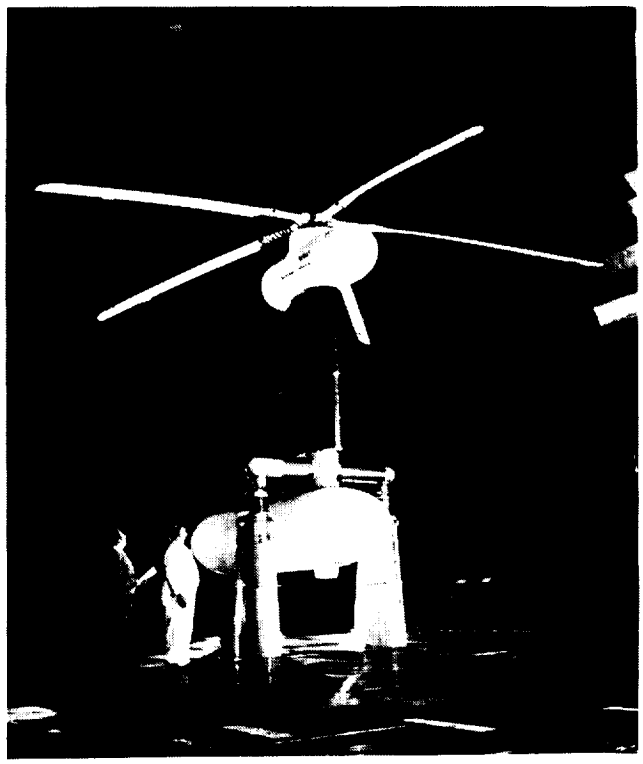

Figure 2. MDART rotor and test stand installed in the 40- by 80-ft test section.

the rotor solidity was 0.075 at sea level standard conditions. More information on the rotor and its development are given in Ref. 7. A more detailed description of the test stand, instrumentation, and data acquisition procedures is presented in Ref. 8.

Instrumentation

The MDART rotor blades, flexbeams, pitchcases, and pitchlinks were instrumented to measure the rotor and control system loads. As indicated in Table 1, flapwise blade bending moments were measured at six radial stations, chordwise blade bending moments at four stations, and blade torsional moments at four stations. The trim tab bending moment was also measured. Pitchcase flap, chord, and torsion moments were measured. The flexbeam had multiple flap, chord, and torsion moment measurements. Single active strain gage measurements were also made at twelve key locations on the flexbeam. All of this instrumentation was located on one arm of the five-armed rotor hub and blade.

The flap, chord, and torsion moments at one location each were also measured on the flexbeam of a second arm, as indicated in Table 1. Flexbeam bending was used to trim the rotor. The rotor was

also instrumented to measure the pitch link load, the bending moment of the swashplate drive scissors, and the effective flap angle.

The shearing displacement of the damper was measured, as were the vertical and horizontal forces at the snubber support. These allowed the effective spring and damping properties of the dampers to be determined.

A five-component rotor balance was used to measure the rotor forces and moments acting on the balance at a location 37 in below the rotor plane Through a series of coordinate transformations, these forces and moments were also expressed as equivalent forces and moments acting at the rotor hub in both the shaft axis and wind axis coordinate systems. The lateral and longitudinal bending moments in the static mast were also measured. The drive shaft was instrumented to measure shaft torque so that the rotor power could be determined.

Table 1. MDART Rotor Instrumentation.

Measurement	Stations (in., ref. from hub center)
Blade Flap Bending Moment	43, 70*, 87, 120, 164, 181
Blade Chord Bending Moment	43, 70*, 120, 164
Blade Torsion Moment	51, 71, 152, 196
Flexbeam Flap Bending Moment	9*
Flexbeam Chord Bending Moment	20*
Flexbeam Torsion Moment	20, 25*
Flexbeam Upper Leg, Leading Edge Strain	Flap: 8, 11, 15 Chord: 8, 11, 15
Flexbeam Lower Leg, Trailing Edge Strain	Flap: 8, 11, 15 Chord: 8, 11, 15
Pitchcase Flap Bending Moment	9
Pitchcase Chord Bending Moment	19.5
Pitchcase Torsion Bending Moment	25
Damper Motion	Displacement*
Flap Sensor	Angular Position
Pitchlink	Axial Strain*
Swashplate Actuators	Force (1 per actuator) Position (2 per actuator)
Main Rotor Balance	Lift, Side & Drag Forces, Pitch and Roll Moments
Rotor Shaft	Torque (2 gages) Bending (2 axes)
Microphones	6 locations
Test Stand Accelerometers	5 locations

* Two measurements from different blades in data base.

Bending bridges on the non-rotating swashplate were used to measure the three actuator loads. Each actuator had dual LVDTs to measure its motion. These measurements were then used to define the collective and cyclic pitch control inputs.

Five microphones were installed in the test section to measure the rotor acoustics. The microphones were placed upstream of the rotor on the advancing side to measure the high-speed impulsive and blade-vortex interaction noise.

Test Matrix

The MDART rotor was tested in hover and at forward speeds of up to 201 kt, with the rotor thrust varied from a few hundred to over 10,000 lb. The test matrix is shown in Fig. 3. Rotor performance and stability data usually were acquired at several shaft angles at each advance ratio and thrust. The stability test matrix is shown in Fig. 4. HHC was tested only at the 1g thrust level (5800 lb) and advance ratios of 0.05, 0.075, 0.20, and 0.30. The airspeeds at which HHC was tested was limited because of the time needed to introduce the many HHC amplitudes and phases.

Most of the test data were acquired with the rotor trimmed to minimize 1/rev flapping. The rotor track was virtually perfect up to 124 kt (μ = 0.30), and then began to split slightly, but never enough to warrant making any tab adjustments. Throughout

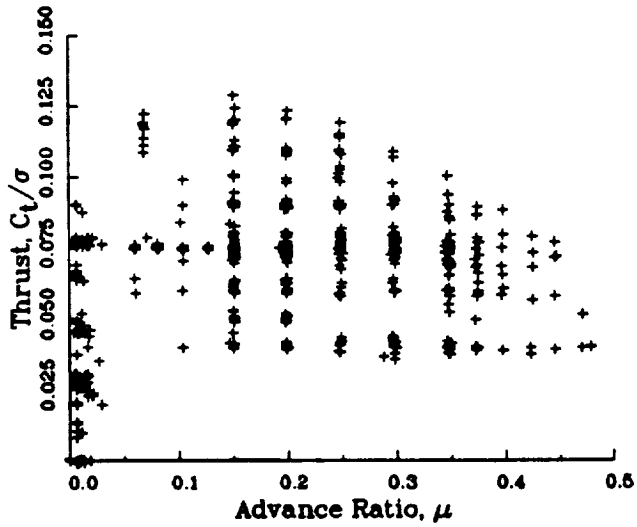

Figure 3: MDART test envelope.

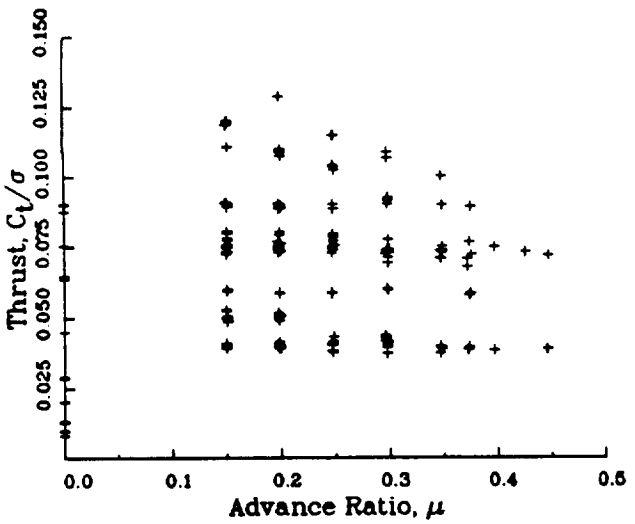

Figure 4: MDART stability test envelope.

the test the rotor operated very smoothly from the standpoint of producing low levels of oscillatory hub loads. The thrusts at most lower airspeeds were limited by the 1000 HP limit of the test stand transmission. At higher airspeeds, the thrust was limited mostly by loads on the flexbeams, pitchcases, and rotor blades.

In addition to the data indicated in Figs. 3 and 4, cyclic control and tip Mach number sweep data were also acquired. To assess the control power of the rotor, lateral and longitudinal cyclic pitch sweeps up to ±2 deg were conducted at the 1g thrust level at advance ratios of 0.15, 0.20, 104, 0.25, and 0.35 kt. The rotor RPM was also varied in hover and at 130 and 157 kt to obtain aeroacoustic data at constant advancing tip Mach numbers of 0.560 and 0.674 (approximately ±10 percent from nominal value of 0.62).

Rotor Performance

Performance Test Method

MDART rotor performance data were obtained over a matrix of advance ratio (μ), rotor shaft angle, and thrust coefficient (C_T). A given data point was obtained while holding rotor shaft angle, collective pitch, rotational hover tip Mach number, and advance ratio constant. As wind tunnel test section air temperature changed, tip Mach number and advance ratio were held constant by adjusting rotor RPM and holding test section dynamic pressure constant. Objectives were to hold advance ratio and Mach number to ± 0.003; this was achieved for most data points. Except for specific Mach number effect investigations, all MDART performance data were taken at a rotational hover tip Mach number of 0.62 (Mach number at 392 RPM at sea-level standard conditions). The performance data were obtained with the rotor trimmed to minimize the first harmonic flapping.

The performance data were measured by the five-component rotor balance and the rotor shaft instrumentation. Rotor performance data are presented in non-dimensional format, scaled by MDART rotor solidity. The data presented have the rotor hub (including pitchcases) aerodynamic tares removed, and are in the wind axis system. Rotor performance data with the hub lift and drag included are available in the MDART data files.

Reference 9, published subsequent to the MDART tests, compares performance results with and without calculated wall corrections for the same 44-ft diameter rotor in both the 40- by 80-ft and 80- by 120-ft test sections. It concluded that wall effects may be neglected for rotor performance for rotors with diameters less than 55 percent of test section width and operating above 0.15 advance ratio. Since this was the case for the MDART data (except for the low speed data discussed below), the rotor shaft angles listed in the data plots herein are the geometric angles, that is, uncorrected for tunnel wall effects.

Flight Performance Results

MDART rotor forward flight performance data was evaluated at advance ratios of 0.15, 0.20, 0.25, 0.30, 0.35, and 0.375. For advance ratio 0.30, Figs. 5 and 6 plot C_L/σ vs. C_Q/σ and C_L/σ vs. C_X/σ for a range of shaft angles, where C_L, C_Q, and C_X are the rotor lift, torque, and drag coefficients, respectively. This data format, which uses the wind tunnel data directly, is convenient for correlating rotor forward flight performance analysis codes with rotor wind tunnel data.

To facilitate calculation of helicopter rotor level flight performance from the MDART data, the data were cross-plotted to eliminate dependence on rotor shaft angle. The results for an advance ratio of 0.30 are presented in Fig. 7. With this format, rotor torque required in level flight can be read directly from the plots, given airspeed and airframe weight, lift, and drag.

Low Speed Forward Flight Performance

MDART rotor low speed forward flight performance data were obtained at C_L/σ = .075 for several

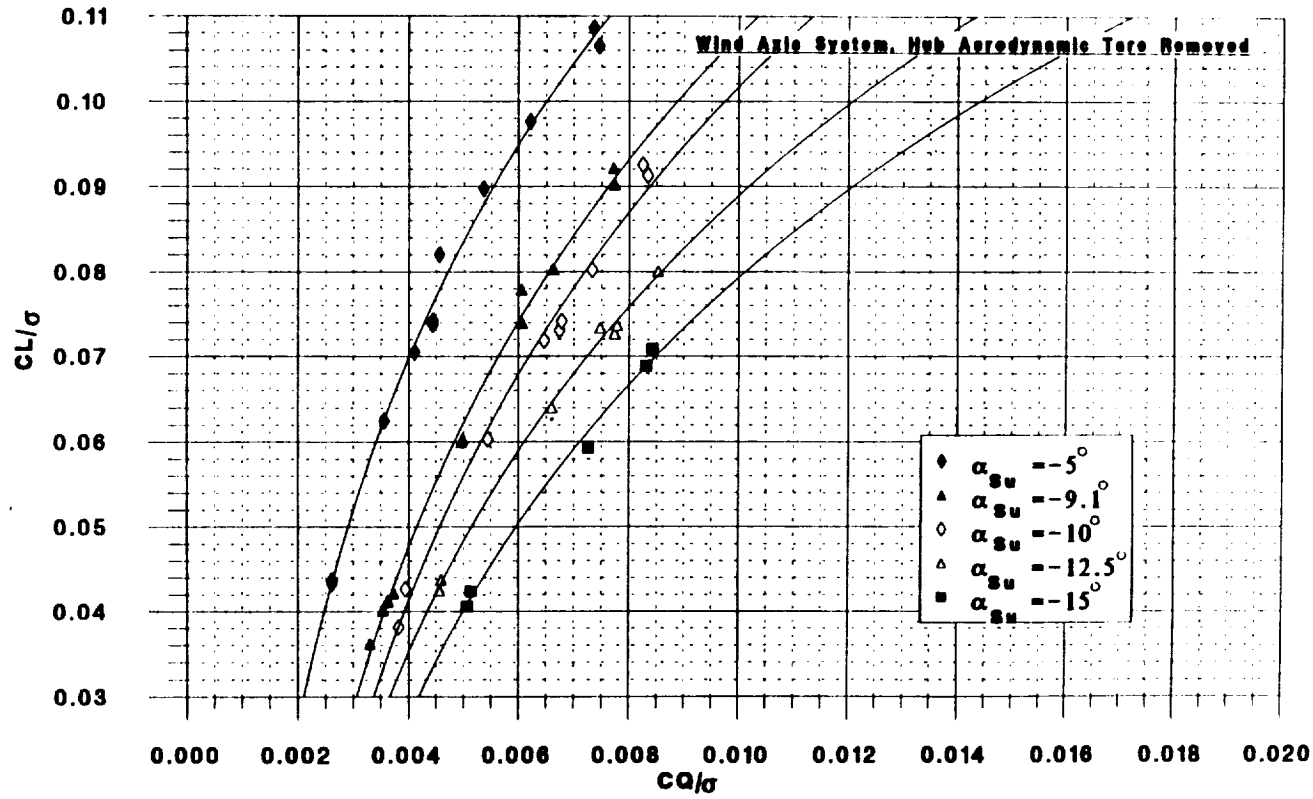

Figure 5: MDART rotor lift vs. torque for advance ratio 0.30.

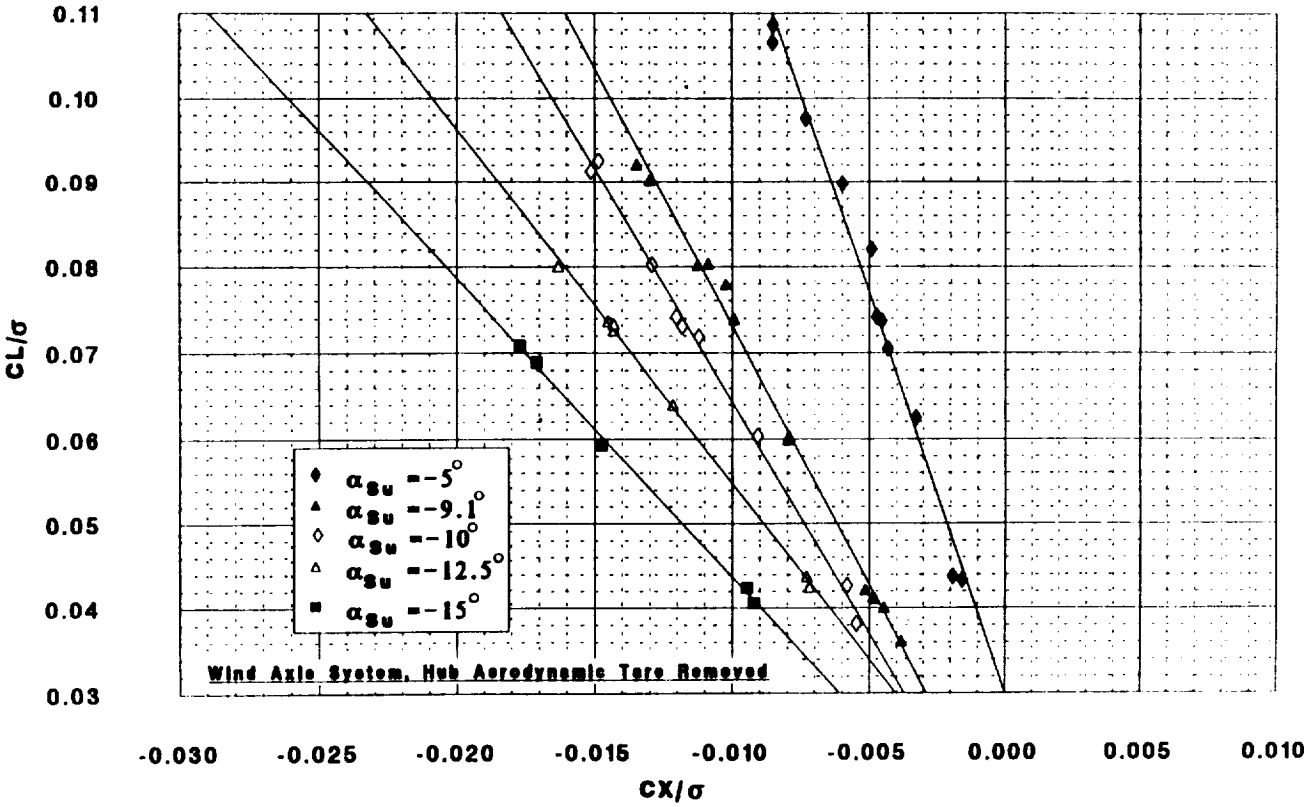

Figure 6: MDART rotor lift vs. propulsive force for advance ratio 0.30.

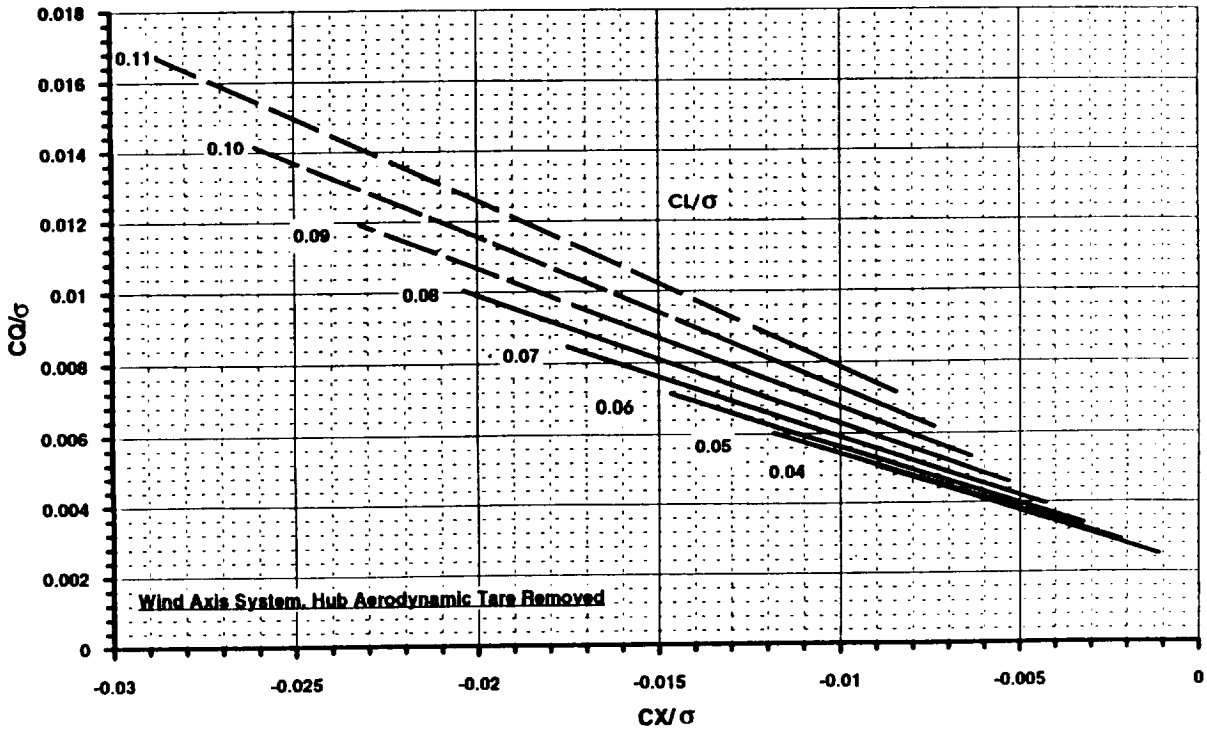

Figure 7: MDART torque vs. lift and propulsive force for advance ratio 0.30.

advance ratios from .06 to .20; the data are presented in Fig. 8. The data for each advance ratio are well fitted by a straight line:

$$C_Q / \sigma = A + B(C_x / \sigma)$$

This relationship agrees with rotor performance theory as developed from energy considerations (e.g., Ref. 10, page 134):

$$C_Q / \sigma = (C_T / \sigma)^2 \left(\frac{\sigma}{2\mu e} \right) + \left(\frac{f}{2\sigma A_R} \right) \mu^3$$

$$+ c_d (1 + 3\mu^2)$$

since for fixed C_T/σ and for a given μ, only the second term (parasite power) varies with C_X/σ:

$$(C_Q / \sigma)_p = \left(\frac{f}{2bcR} \right) \mu^3$$

Since the propulsive force coefficient is given by

$$C_X / \sigma = \left(\frac{-f}{2bcR} \right) \mu^2$$

then

$$C_Q / \sigma = A - \mu (C_X / \sigma)$$

Thus, from energy considerations, the coefficient of C_X/σ for each curve in Fig. 8 should be equal to $-\mu$. The deviation from this ideal value is due to the rotor's propulsive efficiency being less than 100 percent. The ratio of the ideal coefficient to the measured coefficient is the propulsive efficiency (Table 2).

Since η_p greater than 1.0 is not physically possible, the rotor performance data for μ=.06 in Fig. 8 are not correct. This is probably due to large tunnel wall (actually, floor) effects at very low speeds. However, it is concluded from the reasonable and steady values of η_p that the rotor performance data for the other advance ratios in Fig. 8 are valid.

Table 2. Rotor Propulsive Efficiency.

μ	B	$\eta_p = -\mu / B$
0.20	-0.2246	0.89
0.15	-0.1767	0.85
0.127	-0.1475	0.86
0.104	-0.1240	0.84
0.080	-0.0937	0.85
0.060	-0.0449	1.38

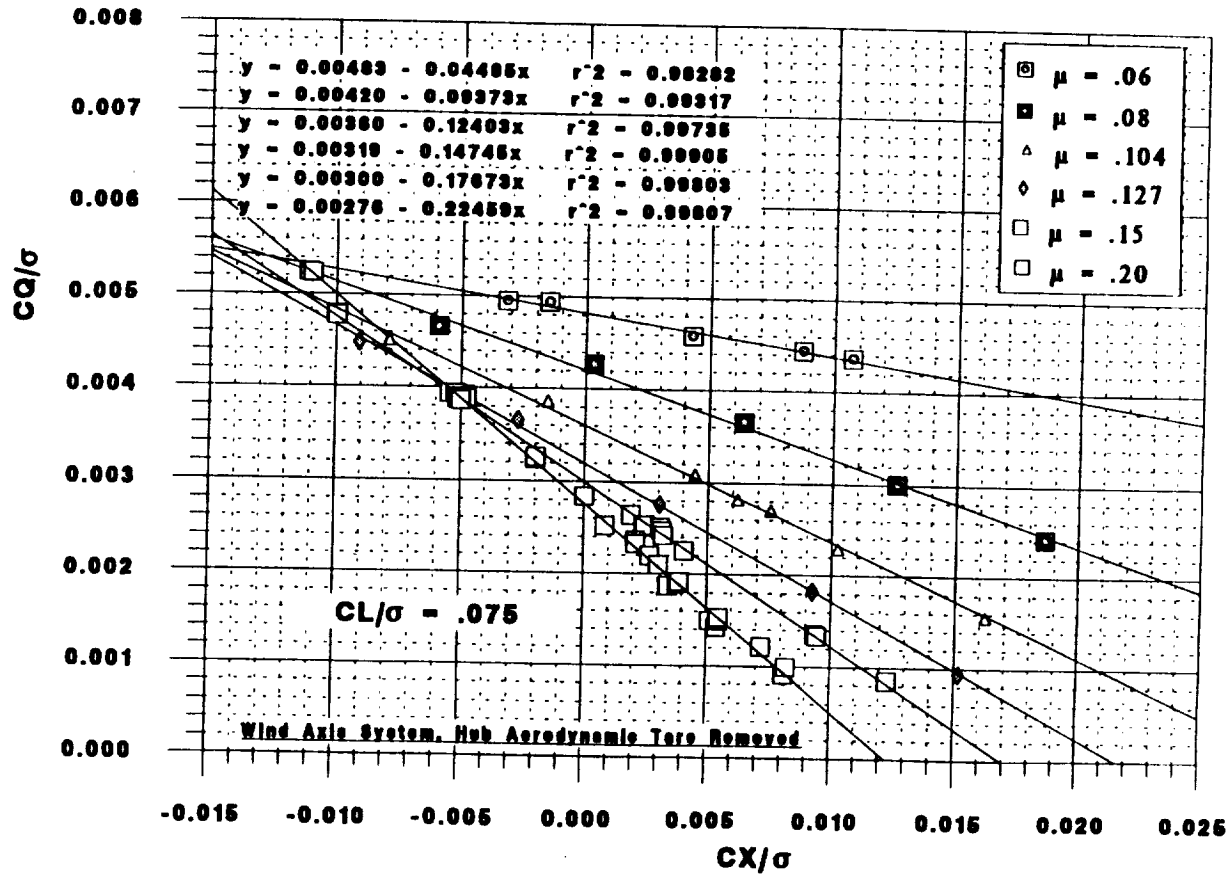

Figure 8: MDART rotor low-speed performance at $CL/\sigma = 0.075$.

Tip Mach Number Effects

The effect of tip Mach number on MDART rotor performance was briefly investigated at $\mu = 0.35$. For a given shaft angle, data were taken at rotational Mach numbers M_H of 0.67 and 0.56 (advancing tip Mach numbers of 0.902 and 0.755) for the same collective settings as the nominal case ($M_H = 0.62$, $M_{AT} = 0.835$). The higher Mach number was set by a frequency limit of the model drive system motor - generator set, which resulted in a rotor RPM limit. Thus $M_H = .67$ and $M_{AT} = .902$ do not represent aerodynamic or structural limits of the MDART rotor.

Because wind tunnel air temperature cannot be controlled to set specific Mach number values, tip Mach number variations for rotor tests are accomplished by varying rotor RPM. Then, to maintain constant advance ratio, tunnel test section dynamic pressure is adjusted. Thus, comparison of C_L/σ vs. C_Q/σ and C_L/σ vs. C_X/σ plots for different tip Mach numbers will not give a true indication of rotor performance trends with M_{AT}. Converting the data to dimensional form does not solve the problem either, for the same reasons. Therefore, a non-dimensional rotor torque coefficient was used which is proportional to rotor shaft horsepower per square foot of blade area, for a given air density and speed of sound:

$$\left(\frac{M_{AT}}{1+\mu}\right)^3 C_Q/\sigma \quad ,$$

where

$$\frac{HP}{bcR} = \frac{\rho V_{sound}^3}{550}\left(\frac{M_{AT}}{1+\mu}\right)^3 C_Q/\sigma \quad .$$

The derivation of this relationship is given in Ref. 11. Similar coefficients for rotor lift and propulsive force are

$$\frac{L}{bcR} = \rho V_{sound}^2\left(\frac{M_{AT}}{1+\mu}\right)^2 C_L/\sigma$$

$$\frac{X}{bcR} = \rho V_{sound}^2\left(\frac{M_{AT}}{1+\mu}\right)^2 C_X/\sigma$$

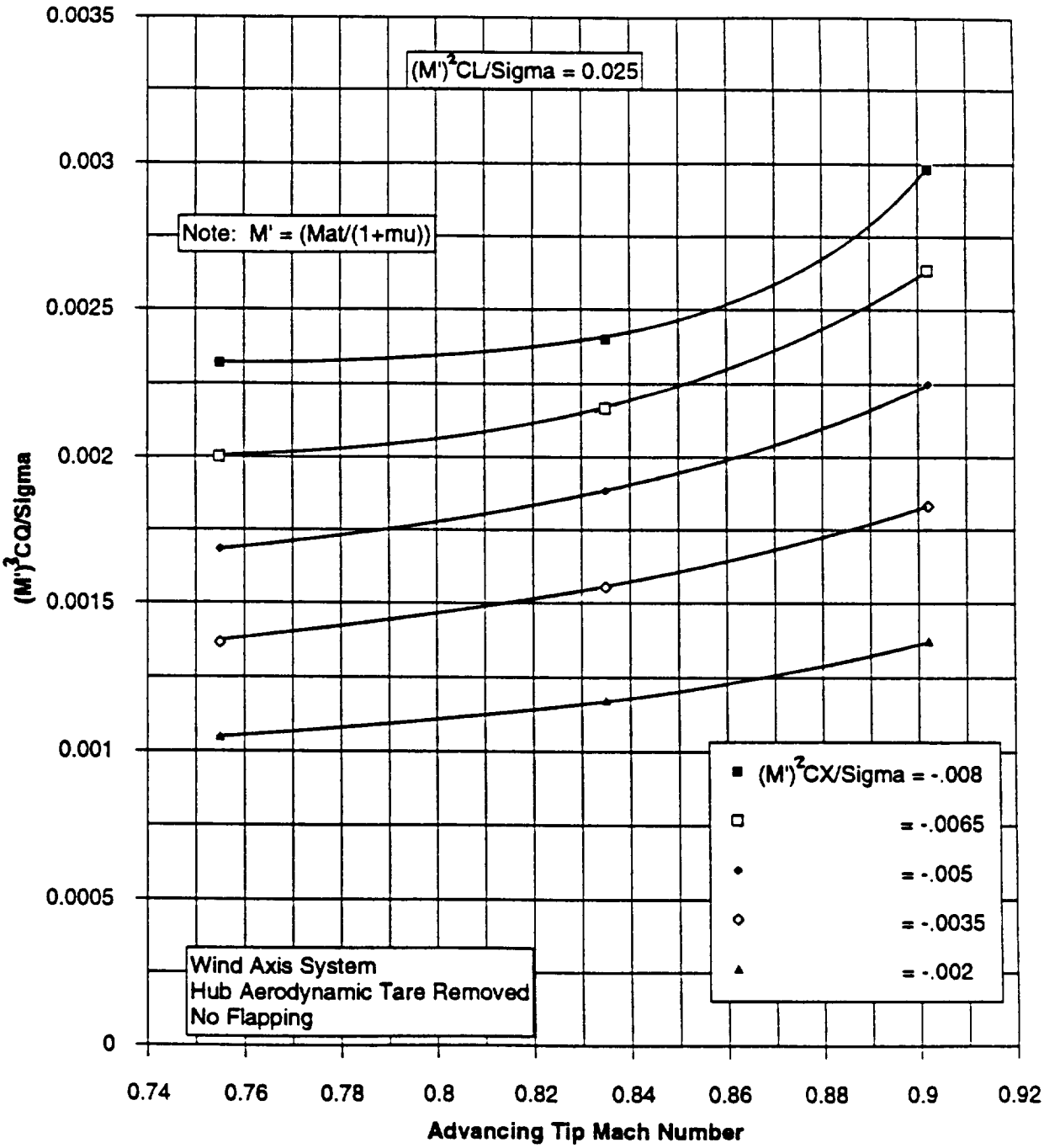

Figure 9. Effect of tip Mach no. on torque coefficient, $(M')^2 CL/\sigma = 0.025$.

Using these modified rotor performance coefficients, plots of torque coefficient vs. advancing tip Mach number for several values of the lift and propulsive force coefficients were prepared. One plot is shown in Fig. 9, where, for convenience, the definition

$$M' = \left(\frac{M_{AT}}{1+\mu} \right)$$

was made. In this plot, a given ordinate increment represents a constant rotor shaft power increment at any M_{AT} and μ combination, for a given air density and speed of sound. Thus these curves may be used to estimate incremental MDART rotor torque due to blade tip Mach number variations. Presumably such increments would be representative of Mach effects for other rotors with similar blade tip thickness and sweep.

Aeroelastic Stability Testing

Aeroelastic stability testing formed an integral part of the MDART test program and was conducted during the expansion of the test envelope. The behavior of the fundamental lead-lag mode dominated the aeroelastic stability of the rotor system. The coupling of this mode, in the fixed system, with the in-plane hub motions could cause dynamic instabilities known as ground and air resonance. The MDART rotor was found to be stable for all wind tunnel conditions tested, and the minimum damping of the blade lead-lag mode was determined to be one percent of critical at the low collective pitch range.

Stability data were acquired by exciting the swashplate actuators at the frequency of the regressive lead-lag mode. The amplitude of the swashplate excitation was raised to a predetermined value or until a load limit condition was reached at any of the instrumented blade stations. The data acquisition, which included the flexbeam chordwise bending strain gauge signal at the 9.6 percent blade radial station and the damper in-plane displacement signal, began shortly before the termination of the excitation. The decay time histories of the signals were then analyzed using a moving block method and a time domain transient analysis method to yield the damping estimates of the blade lead-lag mode. Taking two data points at each condition, application of both estimation algorithms yielded four damping estimates. The transient analysis method [Ref. 12] provided somewhat better damping estimates than the moving block method [Ref. 13] for transient decay records having high damping levels or having small frequency separations between the lead-lag and test stand modes. The damper motions consistently indicated higher damping levels and had more scatter than did the chordwise bending signals. The difference in the damping estimates between two measurements on the same structure was attributed to the nonlinear behaviors of the rotor blade lead-lag dampers. More detailed information on the stability testing methods and the results from the test are contained in Ref. 14.

The aeroelastic database consisted of 277 stability data points covering roughly 140 different test conditions. Stability data were acquired for both hover and forward flight conditions and included RPM sweeps, and thrust and propulsive force sweep at different airspeeds. Sample stability results are shown in Figs. 10 and 11. The data shown are the damping estimates of the blade lead-lag mode obtained using the transient analysis of the flexbeam chordwise bending signal. Figure 10 shows the damping variations with collective pitch in hover, and Fig. 11 shows the damping variation with forward speed at the nominal 1g thrust level (C_T/σ = 0.075).

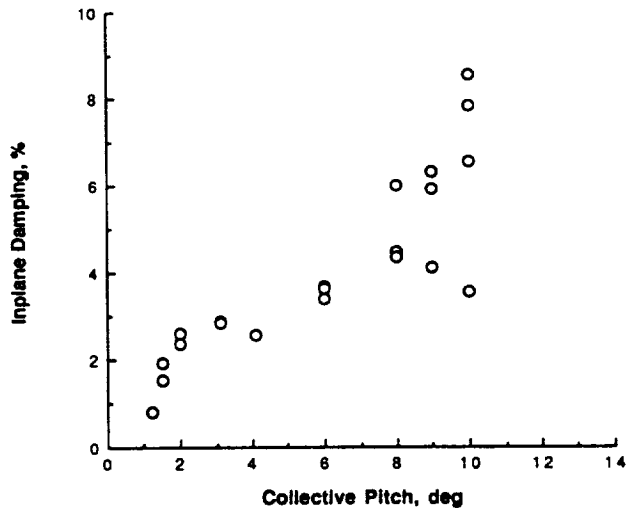

Figure 10. MDART in-plane damping in hover, collective pitch sweep.

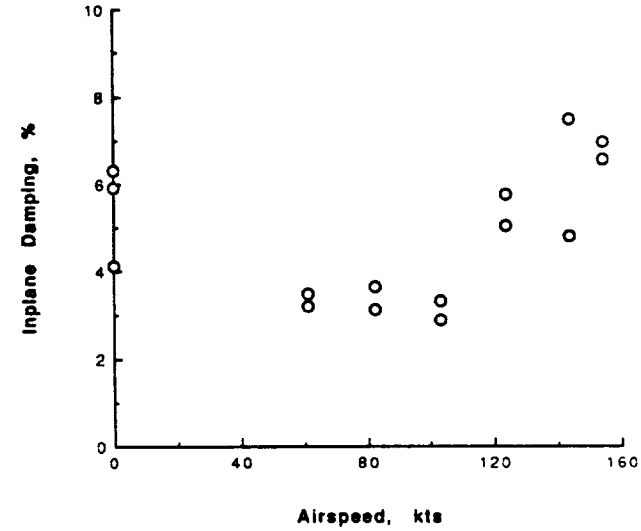

Figure 11. MDART in-plane damping, speed sweep at C_T/σ = 0.075.

Rotor Loads

Computer programs such as the McDonnell Douglas DART code and the University of Maryland UMARC code have been used to predict bearingless rotor loads. These codes attempt to model the redundant load paths which make the load prediction task so difficult. The MDART rotor test acquired an extensive loads database to help validate and enhance the development of codes for bearingless rotors.

Full-bridge strain gage data were acquired at a number of locations on the flexbeam, pitchcase, and rotor blade as previously indicated in Table 1. Single active strain gage data was acquired for several locations on the flexbeam. These gages provided verification of localized strain fields on the beam.

As a sample of the data obtained, Figs. 12 and 13 show the mean flap and mean chord bending moments at 155 kt (μ = 0.375) for a 1-g thrust (C_T/σ = 0.075). Also shown on these plots are load predictions made by DART. Figure 12 shows that the predicted and measured flap bending loads were in good agreement, especially for the blade section. However, Fig. 13 shows that the chord bending was under predicted for the pitchcase and flexbeam, and over-predicted for the blade section for the same condition.

Rotor Control Power

The MDART rotor hub control power was studied by performing lateral and longitudinal control input sweeps at airspeeds of 62, 82, 103, 123, and 143 kt. Data were acquired for longitudinal cyclic input sweeps of up to ±2.0 deg and lateral cyclic input sweeps of up to ±1.0 deg. Though the thrust of the rotor was near 1g, the thrust level was not re-trimmed after each cyclic input.

The changes in pitching moment at the hub (as calculated from the rotor balance data) produced by changes in the longitudinal cyclic input are shown in Fig. 14. Figure 15 shows the effect of changes in the lateral cyclic input on the mean hub rolling moment. For the most part, the data indicated that the hub moment coefficient was relatively invariant with airspeed.

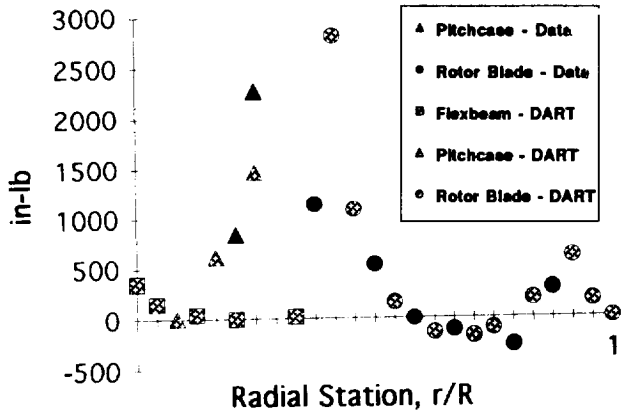

Figure 12. Comparison of predicted and measured mean flap bending at 155 kt.

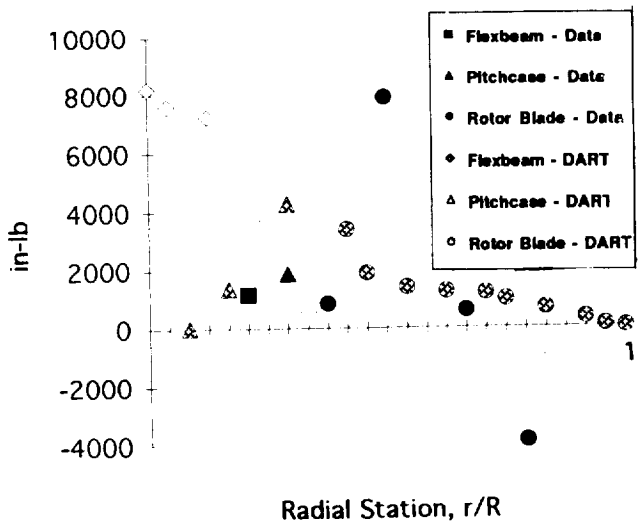

Figure 13. Comparison of predicted and measured mean chord bending at 155 kt.

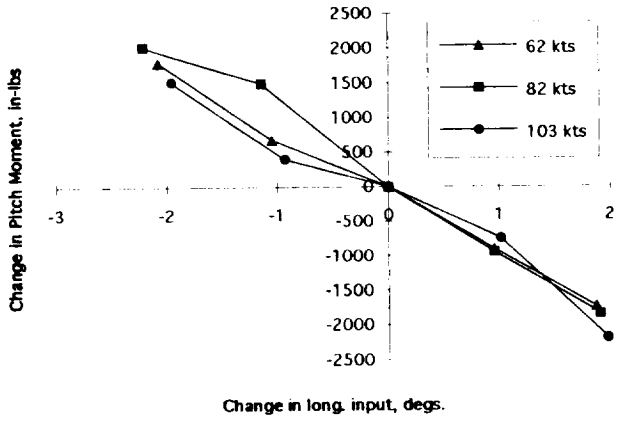

Figure 14. Effect of longitudinal cyclic input on mean hub pitching moment.

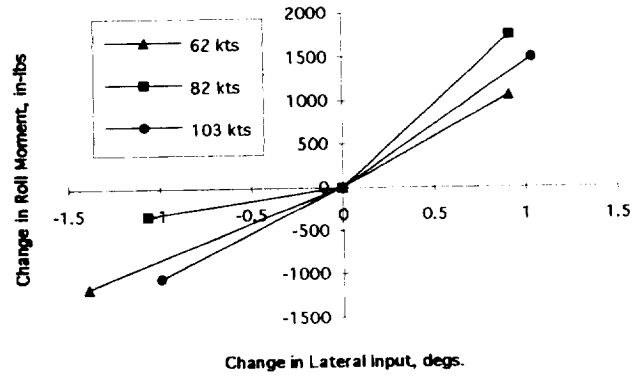

Figure 15. Effect of lateral cyclic input on mean hub rolling moment.

For the case of changes in the longitudinal cyclic pitch input, Figs. 16, 17, and 18 show that very little roll cross-moments were generated. These plots show that when the longitudinal cyclic input was changed, the result was almost a pure change in pitching moment. The slope of each plot is roughly the same; the difference attributed primarily to undesired changes in rotor thrust and trim changes.

In terms of overall control properties, the MDART rotor was very well behaved. The flexbeam geometry and stiffness were tailored to allow the required blade flap, lag, and pitch motions while keeping the first flapping frequency at approximately 1.05/rev. Obtaining a flap frequency this low with a bearingless rotor was a challenging design problem that was solved with optimization techniques [Ref. 15]. The result was a rotor that demonstrated low control cross-couplings and low vibration levels.

Higher Harmonic Control

The MDART rotor test was the first test to apply higher harmonic control (HHC) to a full-scale,

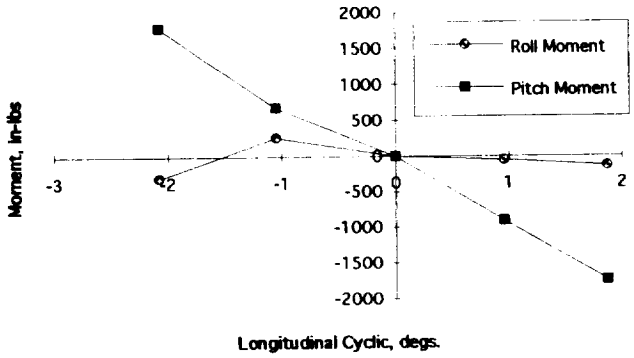

Figure 16. Changes in pitch and roll moment produced by changes in longitudinal cyclic input at 62 kt.

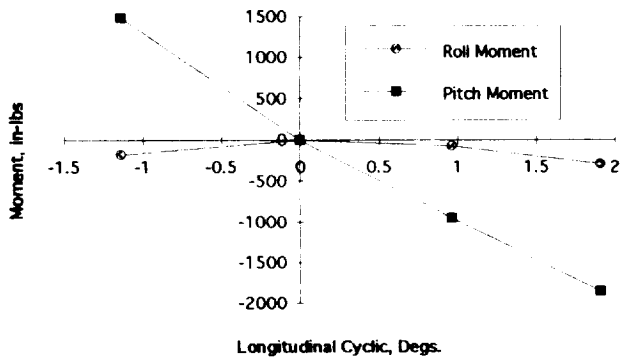

Figure 17. Changes in pitch and roll moment produced by changes in longitudinal cyclic input at 82 kt.

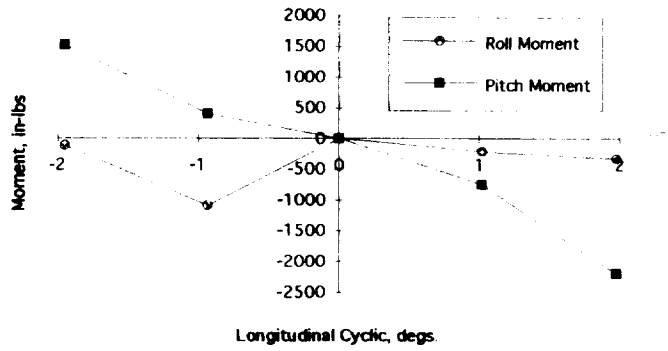

Figure 18. Changes in pitch and roll moment produced by changes in longitudinal cyclic input at 103 kt.

bearingless rotor. This method of rotor control applies small amplitude blade pitch perturbations at integer harmonics of the rotor rotational frequency. Since the MDART rotor was five-bladed, the primary objective was to study the effects of 5-per-revolution (or 5/rev) HHC excitation on the 5/rev vibratory rotor forces and moments. As shown in Fig. 19 for the case of rotor hub pitching moment, the 5/rev vibration harmonic contained most of the vibration energy. This harmonic energy distribution was typical of the other rotor balance forces and moments as well, regardless of flight condition.

The HHC excitation was applied through the swashplate actuators. Though the swashplate actuators were capable of applying 5/rev excitation up to ±1.0 deg, due to excessive loads on the test stand control system, the maximum pitch output was limited to 0.3 deg to 0.5 deg, depending on the phase angle of the input. HHC was introduced at forward flight speeds of 20, 30, 80, and 120 kt. The 80 kt data included both a forward shaft angle tilt typical of level flight at 1g thrust and an aft-tilted shaft to simulate a blade-vortex interaction descent condition. The phase of the 5/rev excitation was varied in 45 deg increments at 30 and 120 kt, and in 90 deg increments at 20 and 80 kt. The phase was defined by the equation

$$5P\,HHC = A\ \cos\!\left(5\Psi + \frac{\phi}{5}\right)$$

where Ψ was the rotor azimuth angle of the reference blade (0 deg defined aft) and ϕ was the phase angle of the HHC input. The swashplate attitude, whether oscillated in collective, lateral, longitudinal modes, was governed by this basic equation. The phase angle, ϕ, was divided by five so

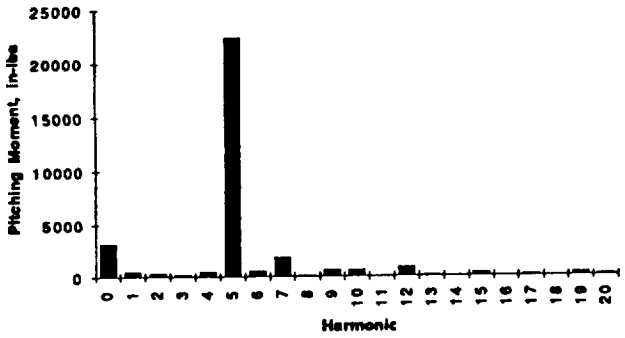

Figure 19. Pitching moment frequency spectrum at 30 kt.

that the phase of the 5/rev control signal relative to the reference would be changed.

Originally, it was intended to introduce pure 5/rev collective, 5/rev lateral, and 5/rev longitudinal HHC. Unfortunately, pure (uncoupled) inputs could not be obtained from the relatively simple HHC control console. Though this did not interfere with calculation of transfer matrices between the control inputs and vibration outputs, it made interpretation of the data more difficult due to multi-parameter input.

To better evaluate the hub load suppression capability of HHC, the hub moments, in-plane forces, and fuselage accelerations are expressed in terms of the performance indices JF, JM, JL, and JA. JF is the vector sum of the 5/rev drag force and 5/rev side force magnitudes. JM is the vector sum of the 5/rev roll moment and 5/rev pitch moment magnitudes. JL is the magnitude of the oscillatory lift force. JA is the sum of vertical, lateral, and longitudinal 5/rev acceleration magnitudes obtained from accelerometers located at one location on the test stand structure.

Figures 20 and 21 show the variation in the 5/rev oscillatory hub moment, oscillatory hub in-plane force, oscillatory lift force, and the fixed-system acceleration location as a function of the HHC inputs for airspeeds of 30 and 120 kt. For each of these quantities, the baseline (no HHC) levels have been plotted as horizontal lines. The rotor was trimmed to minimize 1/rev flapping for all 5/rev inputs. The HHC inputs are labeled as being either "mostly" collective, lateral, or longitudinal. Appendix A presents a table listing the exact input magnitudes and phases keyed to the numbers on the horizontal axes. This table has been included to show that the term "mostly" has been used very loosely. For example, although point 5 in Fig. 20 is grouped under the category of being mostly collective, the entries in Appendix A shows this command to contain an equal amount of lateral 5/rev HHC as well.

HHC was studied at 30 kt and a shaft angle 2.5 deg forward because that condition was found to produce the highest vibration encountered in the transition airspeed region from hover to forward flight. Examination of Fig. 20 shows that the oscillatory 5/rev rotor forces and moments and fuselage accelerations appeared to vary together as the HHC commands were changed.

At 120 kt (μ = 0.30), Fig. 21 shows that the effect of HHC was still very evident, but that the four performance indices were minimized at different phase angles. Note that the level of oscillatory 5/rev hub force and moment vibration generated at the higher airspeed was fairly low. Obviously, the HHC command to minimize oscillatory hub loads is different for 30 and 120 kt.

Using the test data, transfer matrices relating the 5/rev HHC inputs to the 5/rev oscillatory hub load outputs were generated using a least squares regression analysis [Ref. 16]. These transfer matrices were defined by the global model,

$$Z = [T]\theta + Z_0$$

where T is the transfer matrix. Z represented a column vector whose elements were the 5/rev magnitude and phase components of the rotor balance side force, drag force, lift force, roll moment, and pitch moment. θ represented a vector of the 5/rev magnitude and phase components of the collective, lateral, and longitudinal 5/rev HHC. Z_0 represented the baseline hub loads for no HHC. Both T and Z_0 were identified. Transfer matrices were calculated for each airspeed at which HHC was introduced and are presented in Ref. 6. The transfer matrices were seen to vary significantly with airspeed.

Using these transfer matrices and the identified uncontrolled vibration vector, the optimal, open-loop control, θ^*, was calculated by the minimum variance control law,

$$\theta^* = -\left[T^T T\right]^{-1} T^T [Z_0]$$

where T represents the transfer matrix. This control law is a special form of the general result presented in Ref. 17 for the case of an unweighted vibration control performance index with no limiting of control magnitude or control rate. The optimal control inputs were calculated for the 30 and 120 kt

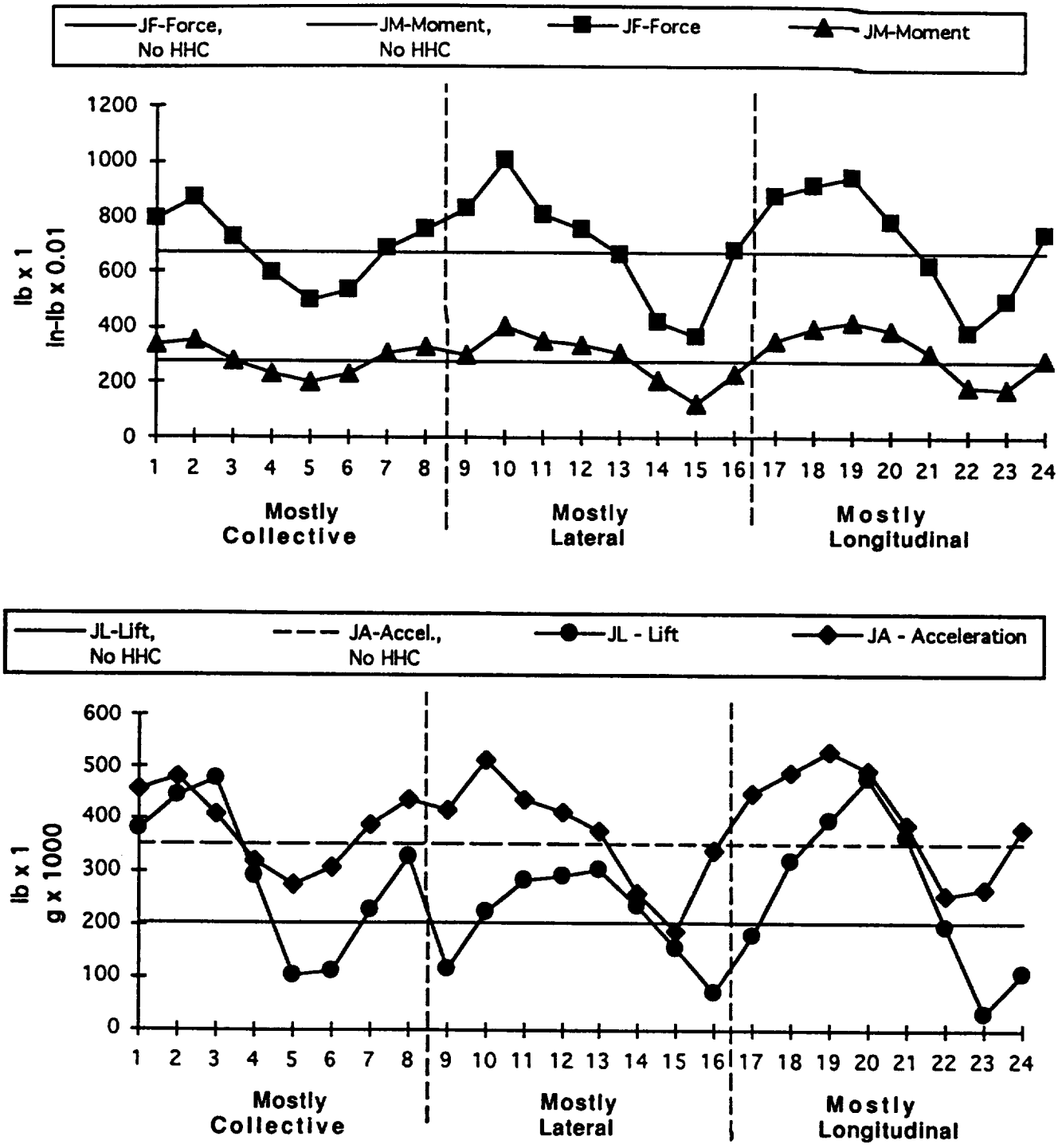

Figure 20. Effect of 5/rev HHC on oscillatory hub forces, hub moments, and fuselage accelerations at 30 kts.

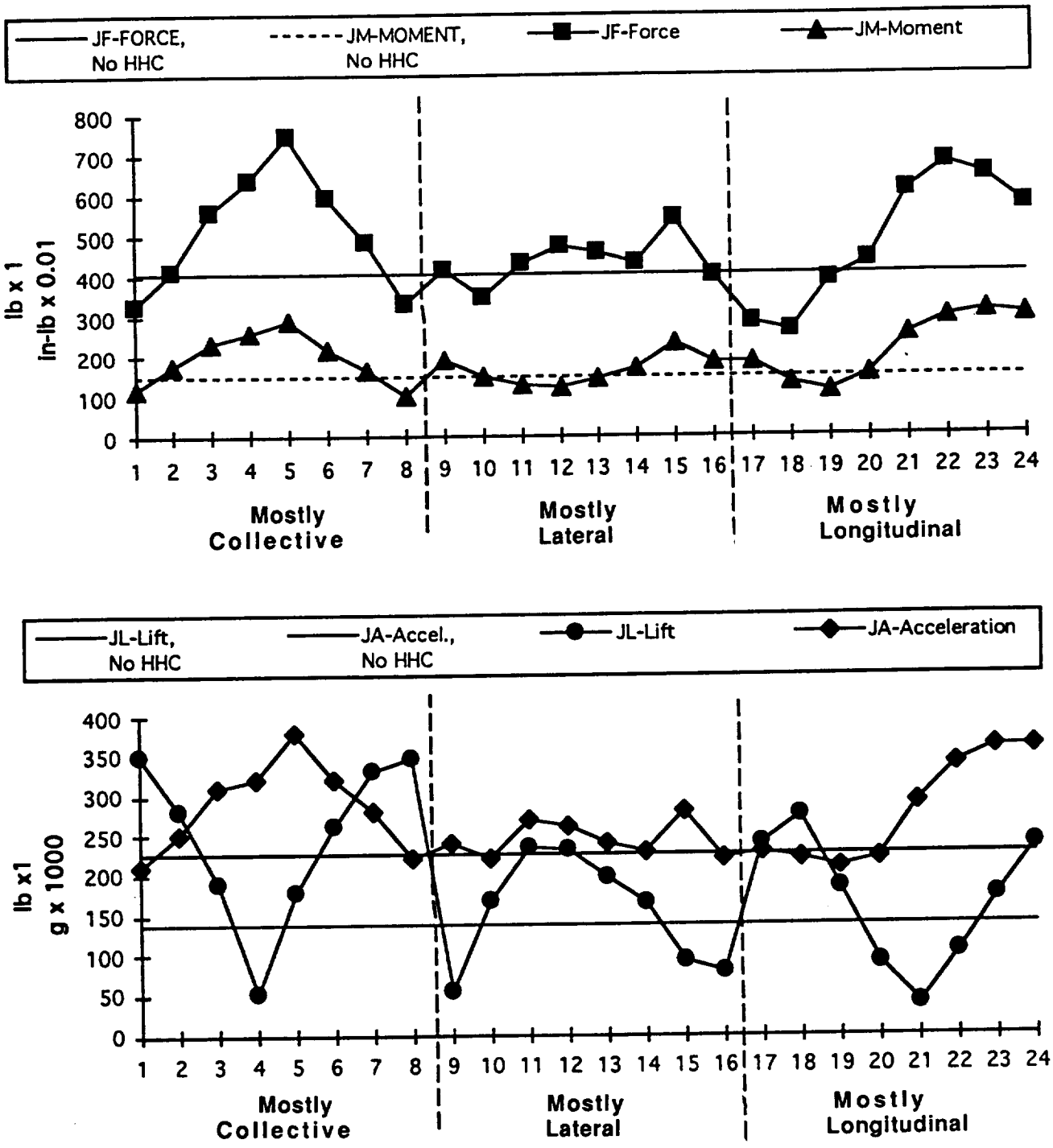

Figure 21. Effect of 5/rev HHC on oscillatory hub forces, hub moments, and fuselage accelerations at 120 kts.

test conditions. Whereas the optimal amplitudes of about 0.3 deg were calculated for 30 kt, 0.8 deg were calculated for the 120 kt condition. Since the optimal control amplitude for 120 kt was outside the range of amplitudes tested, the result might not be valid if the effect of HHC on hub load reduction were significantly nonlinear with input amplitude.

Using these low amplitude controls and the derived transfer matrices, a 5/rev hub moment suppression of better than 95 percent was predicted. The suppression of the 5/rev lift and 5/rev in-plane forces, though, was predicted to be only about 60 percent. However, by weighting the forces more heavily in the optimal control calculation it is expected that a trade-off between the numerically large hub moments and the relatively small in-plane forces could be produced to yield a more even suppression of all hub 5/rev forces and moments.

Effect of HHC on Rotor Power

The effect of HHC on rotor power was calculated from the rotor torque measurement. No significant improvement in rotor performance was expected to be seen during the MDART testing. As discussed in Ref. 18, up to a 10 percent reduction in rotor horsepower could have been expected. Moreover, the reduction in horsepower cited in Ref. 18 was relatively independent of the type of excitation applied. As shown by Fig. 22, the rotor power measured from the shaft torque during the MDART test did not show a 10 percent reduction in power with HHC. However, it should also be noted that the amplitude of input was at most only half of that used in Ref. 18. While a slight decrease in horsepower was indicated for collective excitation, a slight increase was noted for longitudinal HHC. Further, these changes in power are of the same magnitude as the expected accuracy of the thrust measurement.

Concluding Remarks

An extensive amount of performance, stability, loads, vibration, rotor control, and HHC data for a modern, five-bladed bearingless rotor were acquired. The rotor was tested over a wide range of operating conditions including speeds of up to 201 kt and thrusts over 10,000 lb. The MDART rotor was found to be stable for all wind tunnel conditions tested. The rotor behavior was judged to be very good in the sense that it had small control cross-couplings and produced low levels of oscillatory hub loads. In the first ever application of HHC to a full-scale, bearingless rotor, the oscillatory hub loads were seen to be significantly reduced. The MDART

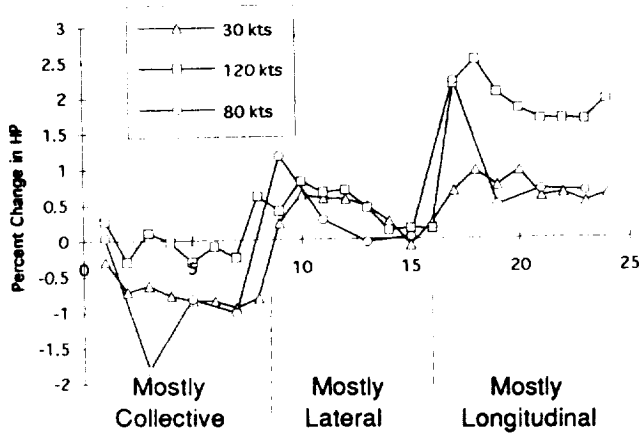

Figure 22. Percent change in rotor horsepower requirements with HHC.

test was a very successful cooperative effort between McDonnell Douglas and NASA. It is hoped that the wind tunnel data obtained will prove useful towards the design and development of future bearingless rotors.

Appendix A

Sample HHC input commands for 30 kt showing amount of control cross couplings. Other airspeeds similar but not identical. See Ref. 6.

Pt.	Commanded 5/rev HHC/Phase	Coll. 5/rev degs	Lat. 5/rev degs	Lon. 5/rev degs
1	Collective, 0°	0.21	0.15	0.02
2	" ", 45°	0.29	0.20	0.06
3	" ", 90°	0.38	0.19	0.15
4	" ", 135°	0.26	0.23	0.08
5	" ", 180°	0.19	0.21	0.06
6	" ", 225°	0.15	0.23	0.06
7	" ", 270°	0.13	0.24	0.05
8	" ", 315°	0.17	0.17	0.03
9	Lateral, 0°	0.07	0.44	0.22
10	" ", 45°	0.07	0.48	0.13
11	" ", 90°	0.07	0.36	0.05
12	" ", 135°	0.08	0.32	0.06
13	" ", 180°	0.11	0.25	0.10
14	" ", 225°	0.11	0.24	0.15
15	" ", 270°	0.11	0.25	0.18
16	" ", 315°	0.08	0.39	0.21
17	Longitudinal, 0°	0.11	0.34	0.20
18	" ", 45°	0.10	0.30	0.23
19	" ", 90°	0.12	0.30	0.31
20	" ", 135°	0.13	0.25	0.59
21	" ", 180°	0.10	0.13	0.51
22	" ", 225°	0.04	0.07	0.48
23	" ", 270°	0.05	0.22	0.37
24	" ", 315°	0.10	0.33	0.30

References

[1] Warmbrodt, W. and McCloud, J., "A Full-Scale Wind Tunnel Investigation of a Helicopter Bearingless Main Rotor," NASA TM 81321, Aug. 1981.

[2] Harse, J., "The Four-Bladed Main Rotor System for the AH-1W Helicopter," American Helicopter Society 45th Annual National Forum, St. Louis, Mo., May 1989.

[3] Von Tein, V. and Schick, C., "BO-108 Technology for New Light Twin Helicopters," 14th European Rotorcraft Forum, Milan, Italy, Sept. 1988.

[4] Norman, T., Cooper, C., Fredrickson, C., and Herter, J. "Full-Scale Wind Tunnel Evaluation of the Sikorsky Five-Bladed Bearingless Main Rotor," American Helicopter Society 49th Annual National Forum, St. Louis, Mo., May 1993.

[5] Dawson, S., et al, "HARP Model Rotor Test at the DNW," American Helicopter Society 45th Annual National Forum, May 1989.

[6] Jacklin, S., Nguyen, K., Lau, B., McNulty, M., and Smith, R., "Full-Scale Test of the McDonnell Douglas, 5-Bladed, Advanced Bearingless Rotor: 40- by 80-Ft Wind Tunnel Data Report," to be published as a NASA TM in 1994.

[7] Murrill, R., Hamilton, B. K., Anand, V. R., Lauzon, D. M., and Tuttle, B., "Bearingless Main Rotor Whirl Test: Design, Analysis and Test Results," American Helicopter Society 49th Annual National Forum, St. Louis, Mo., May 1993.

[8] McNulty, M., Jacklin, S., and Lau, B., "A Full-Scale Test of the McDonnell Douglas Advanced Bearingless Rotor in the NASA Ames 40- by 80-Ft Wind Tunnel," American Helicopter Society 49th Annual National Forum, St. Louis, Mo., May 1993.

[9] Shinoda, P.M., and Johnson, W., "Performance Results from a Test of an S-76 Rotor in the NASA Ames 80- by 120- Foot Wind Tunnel," AIAA Paper 93-3414, AIAA Eleventh Applied Aerodynamics Conference, Monterey, CA, August 1993.

[10] Prouty, R. W., Helicopter Performance, Stability, and Control, PWS Publishers, Boston, 1986.

[11] Charles, B. D., "An Experimental/Theoretical Correlation of Model and Full-Scale Rotor Performance at High Advancing-Tip Mach Numbers and High Advance Ratios," USAAVLABS Technical Report 70-69, January 1971.

[12] Wilcox, P. and Crawford, W., " A Least Squares Method for the Reduction of Free Oscillation Data," NASA TN D-4503, June 1968.

[13] Bousman, W. and Winkler, D., "Application of the Moving Block Analysis," AIAA/ASME/ASCE/-AHS 22nd Structures, Structural Dynamics and Materials Conference, Atlanta, GA, April, 1981.

[14] Nguyen, K., McNulty, M., Anand, V., and Lauzon, D., "Aeroelastic Stability of the McDonnell Douglas Advanced Bearingless Rotor," American Helicopter Society 49th Annual National Forum, St. Louis, Mo., May 1993.

[15] Hamilton, B., Peters, J., and Callahan, C., "Optimal Design of an Advanced Composite Rotating Flexbeam," American Helicopter Society 44th Annual National Forum, Washington, D.C., Jun. 1988.

[16] Jacklin, S. A., "Five System Identification Methods for Higher Harmonic Control", American Helicopter Society 43rd Annual National Forum, St. Louis, Mo., May 1987.

[17] Johnson, W., ``Self-Tuning Regulators for Multicyclic Control of Helicopter Vibration", NASA TP 1996, May 1982.

[18] Wood, R., Platzer, M., Abourahma, A., and Couch, M., "On the Unsteady Aerodynamics of Higher Harmonic Control," Nineteenth European Rotorcraft Forum, Como, Italy, Sept. 1993.